

Article

Relative Stability of Small Silver, Platinum, and Palladium Doped Gold Cluster Cations

Piero Ferrari *  and Ewald Janssens 

Laboratory of Solid State Physics and Magnetism, KU Leuven, 3001 Leuven, Belgium;
ewald.janssens@kuleuven.be

* Correspondence: piero.ferrari@kuleuven.be; Tel.: +32-16-377-503

Received: 31 March 2019; Accepted: 17 April 2019; Published: 23 April 2019



Featured Application: This work uses small single-atom doped gold clusters as model systems for understanding fundamental physical aspects of Ag-Au, Pt-Au, and Pd-Au alloy nanoparticles. Understanding their intrinsic properties is highly desirable in view of better designed bimetallic nanoparticles in catalytic and optical applications with properties that are tuned to meet the requirements of each specific application.

Abstract: The stability patterns of single silver, platinum, and palladium atom doped gold cluster cations, MAu_{N-1}^+ ($M = \text{Ag, Pt, Pd}; N = 3-6$), are investigated by a combination of photofragmentation experiments and density functional theory calculations. The mass spectra of the photofragmented clusters reveal an odd-even pattern in the abundances of AgAu_{N-1}^+ , with local maxima for clusters containing an even number of valence electrons, similarly to pure Au_N^+ . The odd-even pattern, however, disappears upon Pt and Pd doping. Computed dissociation energies agree well with the experimental findings for the different doped clusters. The effect of Ag, Pt, and Pd doping is discussed on the basis of an analysis of the density of states of the $N = 3-5$ clusters. Whereas Ag delocalizes its $5s$ valence electron in all sizes, this process is size-specific for Pt and Pd.

Keywords: metal cluster stability; doping; electronic structure; photofragmentation

1. Introduction

Small metal clusters in the gas phase, produced under conditions where cluster-cluster and cluster-environment interactions are absent, are ideal model systems for a fundamental understanding of the different physical and chemical properties of matter. In a gas phase experiment, clusters are produced and characterized as a function of size, composition, and charge state with atomic precision, and their inherent small size allows for direct comparison with detailed quantum chemical calculations. Many examples in the literature can be found in which small clusters are used to elucidate intrinsic properties of matter, such as the stability of alloy complexes [1,2], the reactivity and catalytic properties of metals [3,4], the optical responses of matter [5,6], and the magnetic coupling of different elements and their evolution from the atom to the bulk [7,8]. In particular, small gold clusters have been intensively studied over the past few decades due to their fascinating properties. For example, at the nanoscale gold becomes reactive towards different molecules [9–12], whereas in bulk it is one of the noblest elements [13]. Moreover, small gold clusters possess unique optical properties [6,14] that are different from those of silver clusters, even though both elements have a similar electronic configuration. The structures of small gold clusters are also remarkable; for instance, Au_{20} is known to adopt a highly symmetric pyramidal geometry [15], and smaller gold clusters remain planar up to surprisingly large sizes. The size at which clusters adopt three dimensional structures in their lowest

energy configuration depends on the charge state. Whereas cationic clusters are planar up to $N = 7$, according to ion mobility experiments [16], anions become three-dimensional at size $N = 12$ [17–19].

The size-dependent stability of small gold clusters is also of interest. In those small metal clusters, each atom delocalizes its $6s$ valence electron over the entire cluster volume. Electron confinement by the small size of the system results in the development of electronic shells with similar nodal character and degeneracy as those in single atoms [20]. Because of the different nature of the confining potential, however, electronic shells in clusters follow a different order, with no restrictions between quantum numbers [21]. The order of the so-called superatomic electronic shells depends on the exact shape of the confining potential, but in spherically symmetric potentials it follows the pattern: 1S, 1P, 1D, 2S, 1F, 2P, ... [22,23]. The filling of these shells explains the famous stability pattern of Na clusters, with intensity maxima at clusters composed of 2, 8, 10, 40, ... atoms [24]. When a cluster has the precise number of atoms, or in this context of delocalized electrons, that close an electronic shell, stability is enhanced with a concomitantly larger energy separation between the highest occupied and lowest unoccupied molecular orbitals (the highest occupied molecular orbital (HOMO)-lowest unoccupied molecular orbital (LUMO) gap) [15]. Such patterns in stability, related to the cluster's electronic shell structure, have been observed mass-spectrometrically in numerous occasions for Au clusters, with a very pronounced size-by-size dependence, since the low-symmetric structures of the clusters lift all but the spin's degeneracy [25–27].

The size-dependency of cluster properties can be greatly altered by the introduction of dopant atoms. This holds for their reactivities [28–30], stabilities [2,31,32], optical properties [14,33], and magnetism [34]. The changes in their properties can be related to an interplay between cluster geometry and electronic structure, both being affected by doping. In the case of gold, the transition at which clusters adopt three-dimensional structures can be largely altered by doping; according to theoretical calculations, for example, a single Pd dopant atom reduces the size at which cationic Au clusters adopt three-dimensional geometries to the smallest possible size of PdAu_3^+ [35]. The electronic structure of a cluster can also be drastically influenced by doping. This is especially the case if the dopant atom has a different number of valence electrons, thus altering the number of itinerant electrons available for filling the superatomic electronic shells [32], or when the dopant atom has a different electronegativity than the host element, inducing significant inter-cluster electron charge transfers [4]. The combination of these effects makes it difficult, a priori, to predict the influence of doping on the stability, even at the very smallest sizes, and requests for a combination of dedicated experiments with theoretical calculations. In this work we combine photofragmentation experiments with density functional theory calculations in order to investigate the effect of doping on the relative stability of small Au_N^+ ($N \leq 6$) clusters. Three dopant atoms have been selected, with electronic configurations slightly different from Au ($[\text{Xe}] 4f^{14} 5d^{10} 6s^1$): Ag ($[\text{Kr}] 4d^{10} 5s^1$), Pt ($[\text{Xe}] 4f^{14} 5d^9 6s^1$), and Pd ($[\text{Kr}] 4d^{10}$).

2. Methods

2.1. Photofragmentation Experiments

Gas phase clusters were produced by laser ablation and inert gas condensation using an experimental setup detailed elsewhere [36]. For the production of M ($M = \text{Ag}, \text{Pt}, \text{Pd}$) doped gold clusters, two independent nanosecond pulsed Nd:YAG lasers (2nd harmonic, 532 nm; Spectra-Physics, Santa Clara, CA, USA) were focused on a gold and an M target, right after a short pulse of He carrier gas (backing pressure of 7 bar) was introduced in the source. By collisions with the carrier gas and subsequent expansion into a vacuum, the ablated plasma condensed and formed a distribution of clusters of various sizes and compositions. This distribution can be tuned by production conditions, including the relative energy of the ablation lasers, their relative firing time, and the pressure of the He gas [37]. In order to obtain information about the relative stability of the clusters, irrespective of the production conditions of the source, the initially charged clusters were electrostatically deflected from the molecular beam and neutral species were excited by a focused excimer F_2 laser

(157 nm). This excitation induces a fast ionization process followed by extensive fragmentation [25]. The abundances of the photofragmented species were then analyzed by time-of-flight mass spectrometry, allowing for the identification of relative stability patterns. This approach has been used in the past to investigate the relative stability of several clusters of different sizes and compositions [27,35,38,39].

For Ag and Pd doping, there was no mass overlap between different species and the different clusters can be easily distinguished in the mass spectra. This is shown in Figure 1, where fractions of typical mass spectra of photofragmented AgAu_{N-1}^+ and PdAu_{N-1}^+ clusters are presented in panels (a) and (b), respectively. Continuous lines connect the MAu_{N-1}^+ species to visualize the size-dependent abundances. This situation is different for the case of Pt doping. Platinum has a distinct isotopic pattern (192 u (0.008%), 194 u (0.329%), 195 u (0.338%), 196 u (0.253%), and 198 u (0.072%)) and the Au atom mass resides in between (197 u). In addition, the strong binding energy of the Pt_2 dimer (4.63 eV compared to 3.15 eV of Au_2 in our calculations) makes it difficult to find production conditions under which only pure Au_N^+ and singly doped PtAu_{N-1}^+ clusters are formed. Thus, pure Pt_N^+ clusters were also produced, as well as mixed $\text{Pt}_x\text{Au}_{N-x}^+$ ($x = 0-N$) species. A part of a typical mass spectrum of the $\text{Pt}_x\text{Au}_{N-x}^+$ clusters is presented in Figure 1c. For this reason, a deconvolution process needed to be performed to quantify the intensity of each cluster composition. An example is presented in Figure 1c. Each $\text{Pt}_x\text{Au}_{N-x}^+$ ($x = 0-N$) intensity profile was assumed to be composed of a set of Gaussian functions matching the natural isotopic distribution of the cluster. The width of a single Gaussian function was determined by recording a mass spectrum of photofragmented pure Au_N^+ clusters (with a single isotope for each size) under the same experimental conditions, in order to account for the mass-dependent resolution of the mass spectrometer. Therefore, the center and the width of each Gaussian function was fixed, while the total intensities of each $\text{Pt}_x\text{Au}_{N-x}^+$ composition were used as fitting parameters. The analysis was restricted to the size range for which this deconvolution could be applied satisfactorily ($N \leq 6$). As a corroboration of the procedure, the extracted abundances of photofragmented pure Au_N^+ and Pt_N^+ clusters were compared with results from previous measurements [35,40], showing an almost identical result.

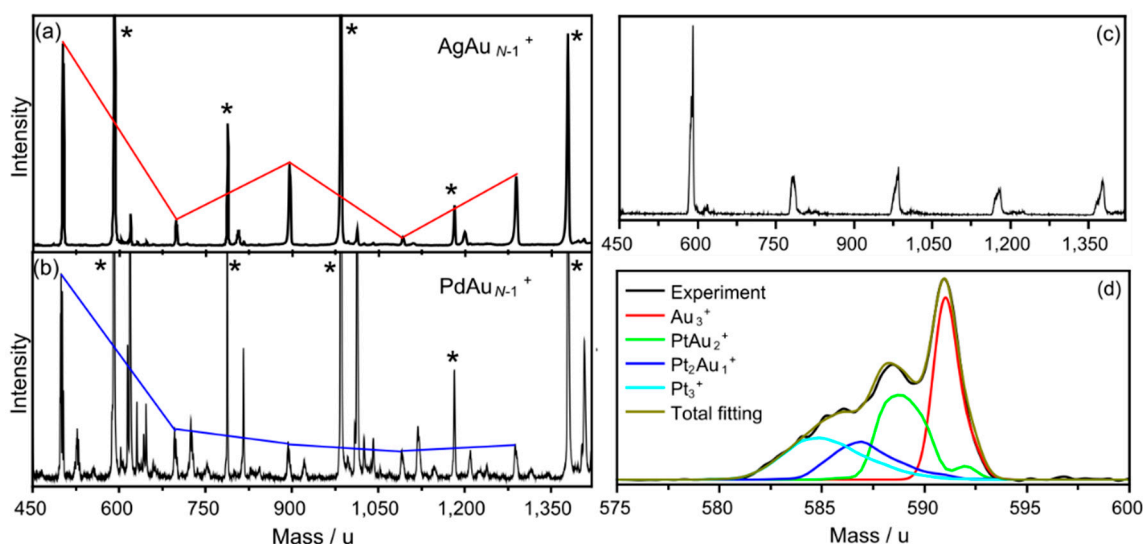


Figure 1. Parts of representative mass spectra of photofragmented clusters: (a) AgAu_{N-1}^+ , (b) PdAu_{N-1}^+ , and (c) PtAu_{N-1}^+ . In (a,b) continuous lines are included to aid visualization of the different abundances of the doped species. Pure Au_N^+ clusters are marked by asterisks, whereas additional peaks correspond to carbon and oxygen contaminations or to doubly doped species of low intensity. (d) Deconvolution of the photofragmented cluster peaks around 580–595 u in panel (c): Au_3^+ , PtAu_2^+ , Pt_2Au_1^+ , and Pt_3^+ . Each peak is assumed to be composed of Gaussian functions of fixed width and matching the natural isotopic distribution of each species.

2.2. Theoretical Calculations

Density functional theory calculations were performed with the ORCA 4.0.1 software package [41]. The lowest energy structures of the clusters were adopted as follows. For the Ag doped clusters, the lowest-energy isomers calculated in Reference [42] were assumed. Experimental characterization of the structures of mixed Au-Ag clusters have been performed up to size $N = 5$ using ion mobility experiments [43], photodissociation spectroscopy measurements [14], and far-infrared multiphoton dissociation studies [44,45]. The structures assigned in these studies agree with those in Reference [42]. For the case of Pt doping, we are not aware of any experimental investigation characterizing the structure of these clusters, nor of a theoretical study searching systematically for low-lying isomers of the cationic species. A search for low-energy structures was performed by manually constructing different initial geometries. Finally, with regards to Pd doping, a thorough theoretical investigation of the Au_N^+ and PdAu_{N-1}^+ ($N = 2-20$) clusters was presented in our previous work [35]. We adopt the structures found there. All geometries were optimized with the LC-BLYP exchange-correlation functional and the extensive Def2-TZVPP basis set [46]. Long-range corrections in Generalized Gradient Approximation (GGA) functionals have been shown to perform well in Pd and Ag doped Au clusters [14,33,35]. In addition, other DFT functionals have been tested, including the GGA PBE, meta-GGA TPSS, and the hybrid B3LYP. For each cluster those other functionals yielded a similar energetic ordering of the considered isomers as the LC-BLYP functional. Additionally, the even larger Def2-QZVPP basis set was checked, showing no significant difference. For these optimizations, the effective core potential Def2-ECP was used, replacing 60 core electrons for Au and Pt, and 28 core electrons for Ag and Pd. For the Ag and Pd doped clusters only the lowest possible spin configurations were calculated, as previous studies showed these have the lowest energy. For the Pt doped clusters, different spin configurations were computed for each cluster size. Also, in this case the lowest possible spin states were found to be the lowest in energy. Vibrational frequencies were calculated for all the structures at the same level of theory to corroborate that the geometries corresponded to true minima on the potential energy surface and not to transition states. Relativistic effects are known to be important for heavy atoms, such as Au and Pt [47]. The cluster sizes investigated here are small enough to allow the implicit inclusion of relativistic effects by performing single point calculations on the optimized structures using the relativistic Hamiltonian within the zero-order regular approximation (ZORA) [48] and the all-electron ZORA-def2-TZVPP basis set [49].

The size-to-size stability of the clusters was analyzed computationally by the dissociation energies D_N , defined as

$$D_N = E(A_{N-m}^+) + E(A_m) - E(A_N^+), \quad (1)$$

where $E(A_N^+)$, $E(A_{N-m}^+)$, and $E(A_m)$ correspond to the total energy of the corresponding cationic clusters and of the emitted neutral fragment. Many theoretical studies make use of another computed quantity when analyzing the relative stability of clusters, namely the second energy difference $\Delta^2 E_N$ [35,40,50,51]. This quantity compares the total energy of size N with that of $N + 1$ plus $N - 1$. Interpretation of experimental data using computed $\Delta^2 E_N$ values, however, requires that the fragmentation channel is always the same, irrespective of the cluster size, or that at least one channel dominates the decay, for example the neutral monomer emission. Recent attempts have even tried to combine D_N and $\Delta^2 E_N$, in order to find a better stability descriptor, by defining a second dissociation energy difference, but this definition requires an invariant fragmentation channel with size [52]. Since here we focus on doped species, the favored channel may be size dependent. Simply comparing the dissociation energies of all possible fragmentation channels is a more solid description of stability and was therefore used in this work.

3. Results

3.1. Abundances of Photofragmented Clusters

The results of the photofragmentation experiments are summarized in Figure 2, which shows the cluster abundances (I_N) for (a) Au_N^+ , (b) AgAu_{N-1}^+ , (c) PtAu_{N-1}^+ , and (d) PdAu_{N-1}^+ clusters, in the size range of $N = 2$ –6. The values of I_N were calculated by integrating the peak area of each corresponding cluster size in the mass spectra. In panel (a) the well-known odd-even oscillation in the abundances of Au_N^+ is seen, with local maxima for clusters composed of an odd number of atoms [25,27,35]. As discussed, this pattern can be understood by the delocalization of each Au 6s valence electron over the cluster volume, which, due to quantum confinement, develops energy shells. The cluster has an enhanced stability if all shells are completely filled. Since these clusters are positively charged, an odd number of atoms corresponds to an even number of electrons, required to close the electronic shells due to spin degeneracy [20]. We point out, however, that this simplified model assumes a negligible influence of the Au 5d electrons on the relative stability pattern.

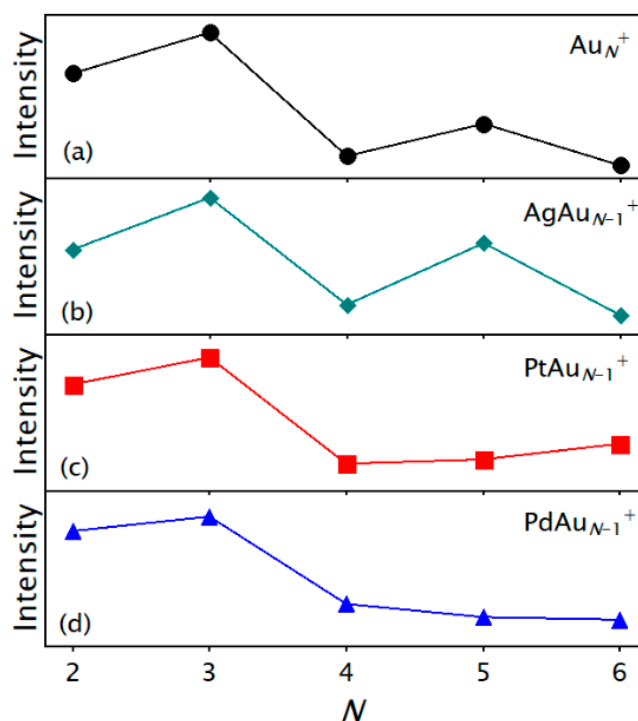


Figure 2. Abundances after photofragmentation for (a) Au_N^+ , (b) AgAu_{N-1}^+ , (c) PtAu_{N-1}^+ , and (d) PdAu_{N-1}^+ clusters; these represent the relative stability of the different sizes. The values were calculated by integrating the area of the corresponding signal in the mass spectra.

Upon Ag doping, as presented in Figure 2b, the odd-even oscillation in the abundances of pure gold clusters was not significantly modified. Local maxima in I_N are found for AgAu_2^+ and AgAu_4^+ , with an amplitude of the abundance oscillation similar to that for pure Au_N^+ . The simple explanation for this is that the silver atom, with an electronic $[\text{Kr}] 4d^{10} 5s^1$ configuration, delocalizes its valence electron for each cluster size. This observation is not surprising, since pure Ag clusters possess a very similar odd-even stability pattern as pure Au clusters [32], although it is slightly more pronounced due to the less influential *d*-states of the clusters in their electronic structure [28].

The effect of Pt doping on the Au_N^+ abundances is shown in Figure 2c. As seen, the odd-even staggering is to some extent preserved upon Pt doping up to $N = 4$, with an intensity maximum at PtAu_2^+ . This pattern, however, changes at $N = 5$, because PtAu_4^+ is not a local intensity maximum. Since the electronic configuration of the platinum atom is $[\text{Xe}] 4f^{14} 5d^9 6s^1$, the observed stability

pattern suggests the delocalization of the Pt 6s valence electron in the $N = 2-4$ size range, giving a total of two delocalized electrons in the PtAu_2^+ cluster. This assumption is not trivial in view of the open d -shell configuration of Pt. An understanding of the modified pattern in the $N = 4-6$ size range upon Pt doping requires further analysis.

Finally, the abundances of the PdAu_{N-1}^+ clusters are shown in Figure 2d. The stability pattern is very similar to that seen for the Pt doped case, with a relative intensity maximum at $N = 3$ but not at $N = 5$. For the Pt doped clusters, this pattern in the abundances suggests that Pd delocalizes one electron in PdAu_2^+ , even though this atom has a ground state electronic configuration with a full d -shell and no valence s electrons ($[\text{Kr}] 4d^{10}$). Photoelectron spectroscopy experiments on anionic PdAu_N^- clusters below $N = 6$ have shown that Pd can promote one of its $4d$ electrons to the $5s$ shell, which then participates in the bonding with Au [53]. In addition, in our previous work on the photofragmentation of larger Pd doped Au cluster cations, we demonstrated similar behavior in PdAu_6^+ [35]. The Pd dopant delocalizes one of its $4d$ electrons, giving to the cluster a total of six itinerant electrons, a pronounced magic number in 2D systems [54]. Therefore, it is possible that Pd is delocalizing an electron in PdAu_2^+ in order to fill the cluster's 1S electronic shell. This assumption, however, requires a detailed analysis of the electronic structure for confirmation. Similarly, further analysis is needed to understand the observation that PdAu_4^+ (as PtAu_4^+) does not seem to possess any particular stability. These matters are discussed later in the text.

3.2. Theoretical Results

The computed lowest energy structures of Au_N^+ and $M\text{Au}_{N-1}^+$ ($N = 2-7$, $M = \text{Ag, Pt, and Pd}$) clusters are shown in Figure 3. The lowest energy structures of cationic Au_N^+ clusters are planar up to $N = 7$ (although Au_7^+ has a slight out-of-plane distortion), according to ion mobility experiments [16]. In many DFT studies, however, it is predicted that the 2D to 3D transition takes place at $N = 8$, although the planar and 3D isomers of Au_8^+ are close in energy [35,55]. The source for this discrepancy can be related to the lack of implicit relativistic effects in most DFT studies on gold clusters, although that question goes beyond the scope of this study. In the $N \leq 7$ size range, theory and experimental results agree that all Au_N^+ clusters are two-dimensional. Upon Ag doping, the 2D-3D transition size is modified. AgAu_4^+ adopts a 3D twisted X-structure, indicating a decrease of the transition size to $N = 5$, but AgAu_5^+ is again a two-dimensional cluster. Pure Ag_N^+ clusters are known to become three-dimensional at $N = 5$, as determined recently by far-infrared multiple photon dissociation spectroscopy measurements in conjunction with DFT calculations [56]. Upon Pt doping, calculations predict the 2D-3D transition at the lowest possible size, i.e., at $N = 4$, with PtAu_3^+ adopting a tetrahedral geometry. Combined far-infrared multiphoton dissociation spectroscopy and DFT calculations have determined that pure Pt_N^+ clusters become three-dimensional at $N = 4$ as well [57], showing the strong tendency of platinum to form 3D structures. For $N > 4$, all cationic Pt doped gold clusters adopt 3D configurations, except for $N = 7$, which maintains the Au_7^+ structure substituting the central Au atom by the Pt dopant (however with a larger out-of-plane distortion). Finally, the case of Pd doping is similar to that of Pt, with 3D geometries from the lowest possible sizes of $N = 4$ onward. For most sizes, except $N = 5$ and 7, the structures of PdAu_{N-1}^+ and PtAu_{N-1}^+ are similar. At $N = 5$, both clusters adopt a 3D twisted X-structure, but the Pt dopant takes the central position of the cluster, whereas the Pd atom is at a side. At $N = 7$ the Pd dopant sits on top of an Au_6 triangular structure which is similar to AgAu_6^+ . The structures of pure Pd_N^+ clusters have not been characterized experimentally. Nevertheless, DFT calculations predict 3D structures from the tetrameric cluster onward, showing also the strong tendency of palladium to adopt 3D configurations [58].

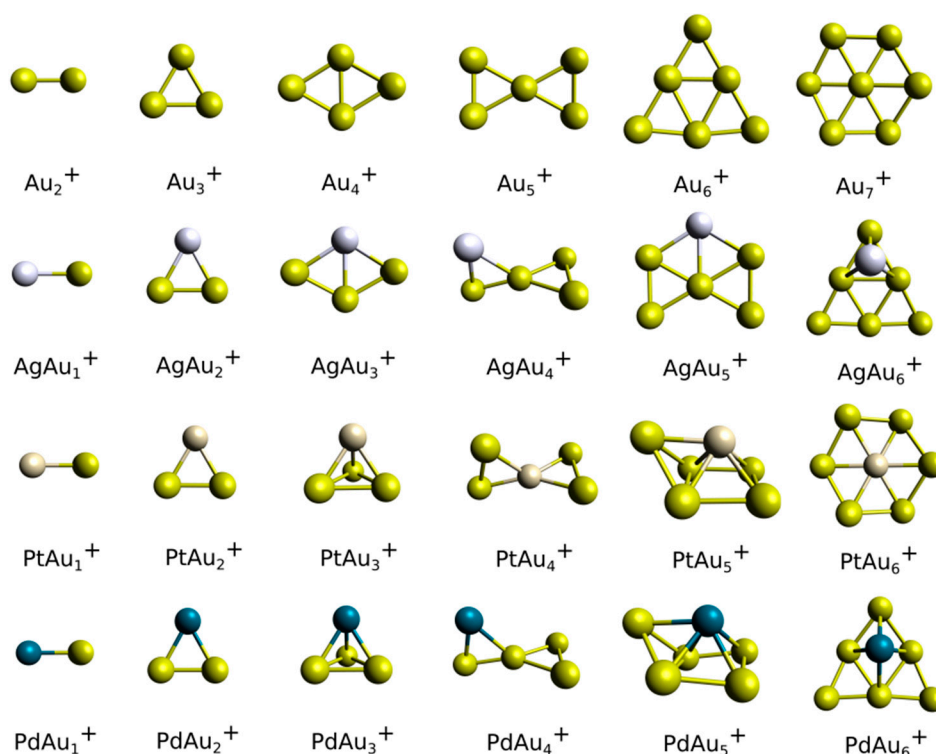


Figure 3. Computed lowest energy structures of Au_N^+ , $AgAu_{N-1}^+$, $PtAu_{N-1}^+$, and $PdAu_{N-1}^+$ ($N = 2-7$).

The computed lowest-energy dissociation channels and the corresponding dissociation energies of Au_N^+ and MAu_{N-1}^+ ($N = 2-7$, $M = Ag, Pt, Pd$) are listed in Table 1. As is known for Au_N^+ , the preferred dissociation channel oscillates between neutral monomer and neutral dimer evaporation, with even(odd)- N clusters preferentially emitting a neutral monomer(dimer) fragment [35,59]. This demonstrates the higher relative stability of Au_3^+ and Au_5^+ since they are in the investigated size range of the preferred daughter clusters. This observation agrees with the interpretation of stability patterns based on valence electron delocalization and electronic shell closing; Au_3^+ has two itinerant electrons, closing the 1S shell, whereas Au_5^+ has four delocalized electrons, closing the 1S shell and the $1P_x$ subshell. The odd-even trend has also been found in experimentally determined dissociation energies of larger Au_N^+ clusters [39]. In Reference [39], D_N values were determined for $N = 7-27$. This range only overlaps with that for Au_7^+ in our work and our computed dissociation energy of 3.20 eV lies within the experimental range of 3.1–3.6 eV. This, however, is only the case after taking into account relativistic effects in the computations. Otherwise, the computed D_N is only 2.90 eV. We also note that a high D_N value was found for Au_3^+ . As mentioned, this cluster has two delocalized electrons, closing the first superatomic shell 1S (more details are given later). Overall, the calculated channels of Au_N^+ agree well with the abundances after photofragmentation, showing higher intensities for Au_3^+ and Au_5^+ .

Table 1. Lowest-energy dissociation channels and corresponding dissociation energies (D_N) of Au_N^+ and MAu_{N-1}^+ ($N = 3-7$, $M = Ag, Pt, Pd$) calculated by density functional theory.

Dissociation Channel		D_N/eV
Au_3^+	$\rightarrow Au_1^+ + Au_2$	4.14
Au_4^+	$\rightarrow Au_3^+ + Au_1$	2.25
Au_5^+	$\rightarrow Au_3^+ + Au_2$	2.58
Au_6^+	$\rightarrow Au_5^+ + Au_1$	2.71
Au_7^+	$\rightarrow Au_5^+ + Au_2$	3.20
$AgAu_2^+$	$\rightarrow Au_1^+ + AgAu_1$	4.69
$AgAu_3^+$	$\rightarrow AgAu_2^+ + Au_1$	2.18
$AgAu_4^+$	$\rightarrow AgAu_2^+ + Au_2$	2.44
$AgAu_5^+$	$\rightarrow AgAu_4^+ + Au_1$	2.51
$AgAu_6^+$	$\rightarrow AgAu_4^+ + Au_2$	3.41
$PtAu_2^+$	$\rightarrow Pt_1^+ + Au_2$	3.97
$PtAu_3^+$	$\rightarrow PtAu_2^+ + Au_1$	3.36
$PtAu_4^+$	$\rightarrow PtAu_3^+ + Au_1$	2.69
	$\rightarrow PtAu_2^+ + Au_2$	2.89
	$\rightarrow Au_3^+ + PtAu_1$	2.91
$PtAu_5^+$	$\rightarrow PtAu_3^+ + Au_2$	2.62
$PtAu_6^+$	$\rightarrow PtAu_4^+ + Au_2$	3.61
	$\rightarrow PtAu_5^+ + Au_1$	3.67
$PdAu_2^+$	$\rightarrow Pd_1^+ + Au_2$	2.83
$PdAu_3^+$	$\rightarrow PdAu_2^+ + Au_1$	3.19
$PdAu_4^+$	$\rightarrow PdAu_3^+ + Au_1$	2.51
	$\rightarrow PdAu_2^+ + Au_2$	2.54
$PdAu_5^+$	$\rightarrow PdAu_3^+ + Au_2$	2.46
$PdAu_6^+$	$\rightarrow PdAu_4^+ + Au_2$	3.32
	$\rightarrow PdAu_5^+ + Au_1$	3.37

Following M heteroatom doping the dissociation patterns can become more complicated, since besides Au_1 and Au_2 evaporation channels, M and MAu_1 emissions can compete. The dissociation energies corresponding to the M and MAu_1 emission channels were computed and with only a few exceptions their energies are significantly higher than those of Au_1 and Au_2 evaporation. For the $AgAu_{N-1}^+$ clusters, a similar pattern to that of Au_N^+ was found; clusters composed of even(odd) numbers of atoms emit a neutral monomer(dimer) gold fragment, thereby preferentially forming $AgAu_4^+$ and $AgAu_2^+$. These two clusters have closed electronic shells with two and four itinerant electrons, respectively, under the assumption that Ag is delocalizing its 5s valence electron. Also, in this case the three-atom cluster, $AgAu_2^+$, has the highest dissociation energy, 4.69 eV, which is actually even higher than that of Au_3^+ . The cases of $PtAu_{N-1}^+$ and $PdAu_{N-1}^+$ are similar but very different from pure Au_N^+ . The clusters MAu_4^+ and MAu_2^+ are not the main products of fragmentation, but instead there is competition to form different daughter clusters in the $N = 3-6$ size range, with some preference for MAu_2^+ . This result is consistent with the experimental observation that there is no special feature in the abundances ($N = 4-6$ size range) of $PtAu_{N-1}^+$ and $PdAu_{N-1}^+$. The underlying reason for this is discussed in the next section.

4. Discussion

The electronic structure of the clusters composed of $N = 3-5$ atoms was analyzed for the different pure and doped clusters via calculations of total density of states (DOS) in order to understand their relative stability. Figure 4 presents this analysis for the clusters composed of three atoms. In the left panel, the DOS of Au_3^+ is shown, which is projected into atomic d -(black) and sp -states (red). Due to the very small size of the cluster, the DOS is composed of molecular-like states with a strong d -character below the HOMO state. Within this dense region of occupied d -states, one state has a higher sp -character (although with an overall low intensity). A plot of the molecular orbital (MO) of this state

shows a wavefunction that is delocalized over the entire cluster, with a nodal character resembling that of the 1S eigenstate of a particle confined in a 2-dimensional potential well [21]. This doubly occupied MO is the only one of delocalized character below the HOMO, showing that Au_3^+ has two itinerant electrons as anticipated. Each of the three Au atoms delocalizes its 6s electron, of which one is removed during ionization. The DOS also reveals the presence of two, almost degenerate, unoccupied MOs resembling the $1P_x$ and $1P_y$ cluster orbitals, which are higher in energy.

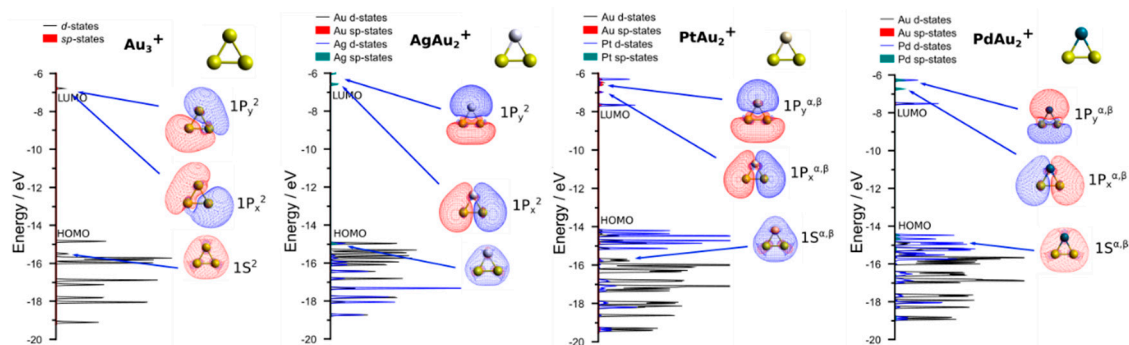


Figure 4. Total density of states of the clusters composed of $N = 3$ atoms. Projections into atomic states are presented in black for Au(d), in red for Au(sp), in blue for M(d), and in green for M(sp). The molecular orbitals of delocalized character extending over the entire cluster volume are plotted and labeled based on their nodal character ($1S$ and $1P_{x,y}$). The highest occupied molecular orbital (HOMO) and lowest unoccupied molecular orbital (LUMO) states are labeled as well. In the case that the cluster is open-shell, both α and β orbitals are plotted.

The second panel of Figure 4 presents the case of AgAu_2^+ , in which the DOS is also projected into the d - (blue) and the sp -states (green) of the silver dopant. The DOS of this cluster is very similar to that of Au_3^+ , with the region close to the HOMO state having a higher Au than Ag character. This is a consequence of the relativistic nature of gold, which reduces the s - d energy separation [28]. As the figure reveals, this cluster also has only one doubly occupied MO of delocalized character ($1S$ symmetry). Therefore, as expected, Ag is delocalizing its $5s$ electron. The PtAu_2^+ and PdAu_2^+ cases, which are presented in the right panels, are different. In both cases the DOS near the HOMO state is dominated by the d -states of the dopant atom, and, as for Au_3^+ and AgAu_2^+ , only one MO of delocalized character is found to be doubly occupied. This indicates that PtAu_2^+ and PdAu_2^+ are also clusters with closed electronic shells, which is not trivial considering the electronic configuration of these dopant atoms. Therefore, at $N = 3$ the Pt dopant delocalizes its $6s$ electron ($[\text{Xe}] 4f^{14} 5d^9 6s^1$), whereas the Pd dopant ($[\text{Kr}] 4d^{10}$) promotes one of its $4d$ electrons to an electronic configuration of $[\text{Kr}] 4d^9 5s^1$, which then delocalizes over the entire cluster. This leaves both dopant atoms with an open atomic d -shell.

In Figure 5, a similar DOS analysis is presented for $N = 4$. Au_4^+ and AgAu_3^+ have very similar DOS. In both cases the HOMO corresponds to a singly occupied MO of delocalized character (α -state) with the $1P_x$ symmetry. In addition, there is a doubly occupied MO resembling the $1S$ eigenstate. The lowest unoccupied molecular orbital (LUMO) of the clusters is now the β -state of $1P_x$ symmetry. Therefore, Au_4^+ and AgAu_3^+ have three itinerant electrons. The DOS of PtAu_3^+ and PdAu_3^+ is remarkable; both clusters have only the $1S$ -type delocalized MOs below the HOMO, implying that there are in total only two delocalized electrons. As shown in the figure, the $1P_x$ and $1P_y$ MOs are empty. For $N = 4$, neither Pt nor Pd contributes to the electron delocalization, contrary to the $N = 3$ case. PtAu_3^+ and PdAu_3^+ are clusters with closed electronic shells, as PtAu_2^+ and PdAu_2^+ are.

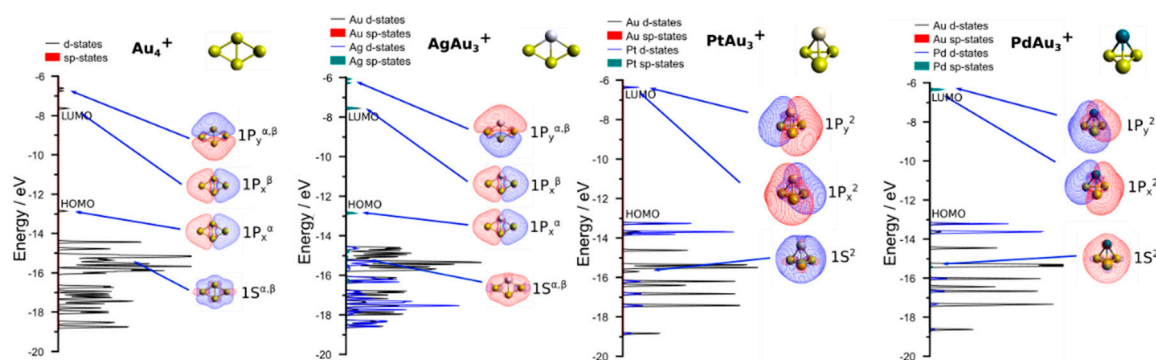


Figure 5. Total density of states of the clusters composed of $N = 4$ atoms. Projections into atomic states are presented in black for Au(d), in red for Au(sp), in blue for M (d), and in green for M (sp). The molecular orbitals of delocalized character extending over the entire cluster volume are plotted and labeled based on their nodal character ($1S$ and $1P_{x,y}$). The HOMO-LUMO gap is labeled. In the case that the cluster is open-shell, both α and β orbitals are plotted.

The final analyzed case (size $N = 5$) is presented in Figure 6. As expected, Au_5^+ and $AgAu_4^+$ are clusters with closed electronic shells, since each atom delocalizes one valence electron. In both cases there are two doubly occupied MOs of delocalized character which resemble the $1S$ and $1P_x$ eigenstates. This is similar to the cases of $PtAu_4^+$ and $PdAu_4^+$, which also have two doubly occupied MOs of delocalized character. For $N = 5$, Pt and Pd delocalize one electron in order to close the $1P_x$ electronic shell of the clusters, thereby gaining stability. This analysis shows an a priori unexpected behavior of the Pt and Pd dopants on the Au clusters in the $N = 3-5$ size range. The dopant atoms delocalize one electron at $N = 3$ and $N = 5$, but none at $N = 4$, allowing all the doped clusters to have closed electronic shells.

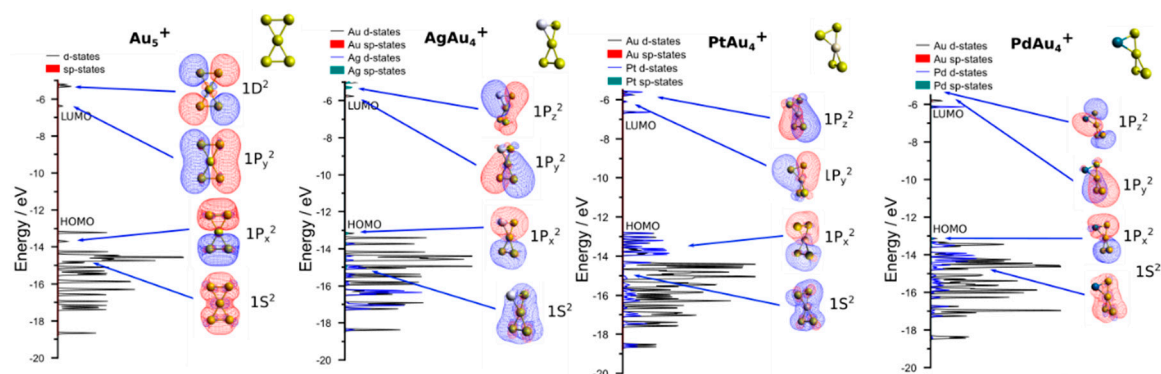


Figure 6. Total density of states of the clusters composed of $N = 5$ atoms. Projections into atomic states are presented in black for Au(d), in red for Au(sp), in blue for M (d), and in green for M (sp). The molecular orbitals of delocalized character extending over the entire cluster volume are plotted and labeled based on their nodal character ($1S$ and $1P_{x,y,z}$). The HOMO-LUMO gap is labeled. In the case that the cluster is open-shell, both α and β orbitals are plotted.

5. Conclusions

In this work, the relative stability of small cationic Ag, Pt, and Pd doped Au_N^+ ($N = 2-7$) clusters were investigated using a combination of photofragmentation experiments and density functional theory calculations. Mass spectra revealed a pronounced odd-even pattern in the abundances of Au_N^+ and $AgAu_{N-1}^+$, which can be rationalized by considering the delocalization of the s -valence electron of each atom in the cluster, including the Ag dopant. Clusters composed of an odd number of atoms possess an even number of delocalized electrons, closing superatomic electronic shells and gaining stability. Dissociation energies calculated for these clusters agree well with this picture, since the

preferred fragmentation channels always produce the more stable fragments: Au_3^+ , Au_5^+ , AgAu_2^+ , and AgAu_4^+ . The Pt and Pd doped clusters, however, behave very differently. Experimentally, PtAu_2^+ and PdAu_2^+ correspond to intensity maxima, but PtAu_4^+ and PdAu_4^+ do not. The calculated dissociation energies of these clusters reveal a competition between channels that produce fragments of different sizes, especially in the $N = 4$ – 6 size range, explaining the smeared out odd-even pattern in their size-to-size dependent abundances. Analysis of the density of states of the clusters in the $N = 3$ – 5 size range reveals an unexpected behavior. At $N = 3$, both Pt and Pd delocalize one valence electron in order to close the 1S superatomic electron shell. At $N = 4$, though, the valence electrons of both dopants remain localized, which also allows the closing of the clusters' 1S shells. Finally, at the size $N = 5$, Pt and Pd again delocalize one electron, closing the 1S and $1P_x$ shells. Overall, these results illustrate that it is difficult to predict a priori how doping would affect the electronic structure of clusters, even at the very smallest sizes.

Author Contributions: Conceptualization, P.F. and E.J.; formal analysis, P.F.; investigation, P.F. and E.J.; resources, P.F. and E.J.; writing—original draft preparation, P.F.; writing—review and editing, P.F. and E.J.; project administration, E.J.

Funding: This research was funded by the Research Foundation-Flanders (FWO) (grant number G0B41.15N) and by the KU Leuven Research Council (grant number C14/18/073).

Acknowledgments: P.F. acknowledges the FWO for a postdoctoral grant.

Conflicts of Interest: The authors declare no conflict of interest.

References

1. Liao, T.-W.; Yadav, A.; Hu, K.-J.; van der Tol, J.; Cosentino, S.; D'Acapito, F.; Palmer, R.E.; Lenardi, C.; Ferrando, R.; Grandjean, D.; et al. Unravelling the nucleation mechanism of bimetallic nanoparticles with composition-tunable core-shell arrangements. *Nanoscale* **2018**, *10*, 6684. [[CrossRef](#)]
2. Neukermans, S.; Janssens, E.; Chen, Z.F.; Silverans, R.E.; Schleyer, P.v.R.; Lievens, P. Extremely Stable Metal-Encapsulated AlPb_{10}^+ and AlPb_{12}^+ Clusters: Mass-Spectrometric Discovery and Density Functional Theory Study. *Phys. Rev. Lett.* **2004**, *92*, 163401. [[CrossRef](#)]
3. Zhou, S.; Li, J.; Schlangen, M.; Schwarz, H. Bond Activation by Metal-Carbene Complexes in the Gas Phase. *Acc. Chem. Res* **2016**, *49*, 494–502. [[CrossRef](#)] [[PubMed](#)]
4. Ferrari, P.; Molina, L.M.; Kaydashev, V.E.; Alonso, J.A.; Lievens, P.; Janssens, E. Controlling the Adsorption of Carbon Monoxide on Platinum Clusters by Dopant-Induced Electronic Structure Modification. *Angew. Chem. Int. Ed.* **2016**, *55*, 11059–11063. [[CrossRef](#)]
5. Philip, R.; Chantharasupawong, P.; Qian, H.; Jin, R.; Thomas, J. Evolution of Nonlinear Optical Properties: From Gold Atomic Clusters to Plasmonic Nanocrystals. *Nano Lett.* **2012**, *12*, 4661. [[CrossRef](#)] [[PubMed](#)]
6. Gloess, A.N.; Schneider, H.; Weber, J.M.; Kappes, M.M. Electronically excited states and visible region photodissociation spectroscopy of $\text{Au}_m^+ \cdot \text{Ar}_n$. *J. Chem. Phys.* **2008**, *128*, 114312. [[CrossRef](#)] [[PubMed](#)]
7. Xu, X.; Yin, S.; Moro, R.; de Heer, W.A. Magnetic Moments and Adiabatic Magnetization of Free Cobalt Clusters. *Phys. Rev. Lett.* **2005**, *95*, 237209. [[CrossRef](#)] [[PubMed](#)]
8. Ngan, V.T.; Janssens, E.; Claes, P.; Lyon, J.T.; Fielicke, A.; Nguyen, M.T.; Lievens, P. High Magnetic Moments in Manganese-Doped Silicon Clusters. *Chem. Eur. J.* **2012**, *18*, 15788. [[CrossRef](#)]
9. Haruta, M.; Yamada, N.; Kobayashi, T.; Iijima, S. Gold catalysts prepared by coprecipitation for low-temperature oxidation of hydrogen and of carbon monoxide. *J. Catal.* **1989**, *115*, 301–309. [[CrossRef](#)]
10. Neumaier, M.; Weigend, F.; Hampe, O.; Kappes, M.M. Binding energies of CO on gold cluster cations Au_n^+ ($n = 1$ – 65): A radiative association kinetics study. *J. Chem. Phys.* **2005**, *122*, 104702. [[CrossRef](#)]
11. Janssens, E.; Le, H.T.; Lievens, P. Adsorption of Propene on Neutral Gold Clusters in the Gas Phase. *Chem. Eur. J.* **2015**, *21*, 15256–15262. [[CrossRef](#)]
12. Lang, S.M.; Bernhardt, T.M.; Barnett, R.N.; Landman, U. Methane activation and catalytic ethylene formation on free Au_2^+ . *Angew. Chem. Int. Ed.* **2010**, *49*, 980–983. [[CrossRef](#)]
13. Hammer, B.; Norskov, J.K. Why gold is the noblest of all the metals. *Nature* **1995**, *376*, 238–240. [[CrossRef](#)]
14. Shayeghi, A.; Heard, C.J.; Johnston, R.L.; Schäfer, R. Optical and electronic properties of mixed Ag-Au tetramer cations. *J. Chem. Phys.* **2014**, *140*, 054312. [[CrossRef](#)]

15. Gruene, P.; Rayner, D.M.; Redlich, B.; van der Meer, A.F.G.; Lyon, J.T.; Meijer, G.; Fielicke, A. Structures of Neutral Au₇, Au₁₉, and Au₂₀ Clusters in the Gas Phase. *Science* **2008**, *321*, 674. [[CrossRef](#)]
16. Gilb, S.; Weis, P.; Furche, P.; Ahlrichs, R.; Kappes, M.M. Structures of small gold cluster cations (Au_n⁺, n < 14): Ion mobility measurements versus density functional calculations. *J. Chem. Phys.* **2002**, *116*, 4094. [[CrossRef](#)]
17. Furche, F.; Ahlrichs, R.; Weis, P.; Jacob, C.; Gilb, S.; Bierweiler, T.; Kappes, M.M. The structures of small gold cluster anions as determined by a combination of ion mobility measurements and density functional calculations. *J. Chem. Phys.* **2002**, *117*, 6982. [[CrossRef](#)]
18. Häkkinen, H.; Yoon, B.; Landman, U.; Li, X.; Zhai, H.-J.; Wang, L.-S. On the Electronic and Atomic Structures of Small Au_N⁻ (N = 4–14) Clusters: A Photoelectron Spectroscopy and Density-Functional Study. *J. Phys. Chem. A* **2003**, *107*, 6168. [[CrossRef](#)]
19. Xing, X.; Yoon, B.; Landman, U.; Parks, J.H. Structural evolution of Au nanoclusters: From planar to cage to tubular motifs. *Phys. Rev. B* **2006**, *74*, 165423. [[CrossRef](#)]
20. Häkkinen, H. Electronic shell structures in bare and protected metal nanoclusters. *Adv. Phys. X* **2016**, *1*, 467–491. [[CrossRef](#)]
21. Atkins, P.W.; Friedman, R.S. *Molecular Quantum Mechanics*, 5th ed.; Oxford University Press Inc.: New York, NY, USA, 2011; ISBN 978-0-19-954142-3.
22. De Heer, W.A. The physics of simple metal clusters: Experimental aspects and simple models. *Rev. Mod. Phys.* **1993**, *65*, 611. [[CrossRef](#)]
23. Reber, A.C.; Khanna, S.N. Superatoms: Electronic and Geometric Effects on Reactivity. *Acc. Chem. Res.* **2017**, *50*, 255–263. [[CrossRef](#)] [[PubMed](#)]
24. Knight, W.D.; Clemenger, K.; de Heer, W.A.; Saunders, W.A.; Chou, M.Y.; Cohen, M.L. Electronic Shell Structure and Abundances of Sodium Clusters. *Phys. Rev. Lett.* **1984**, *53*, 510. [[CrossRef](#)]
25. Veldeman, N.; Janssens, E.; Hansen, K.; De Haeck, J.; Silverans, R.E.; Lievens, P. Stability and dissociation pathways of doped Au_nX⁺ clusters (X = Y, Er, Nb). *Faraday Discuss.* **2008**, *138*, 147–162. [[CrossRef](#)]
26. Hansen, K.; Ferrari, P.; Janssens, E.; Lievens, P. Thermal radiation of gold clusters on microsecond time scales. *Phys. Rev. A* **2017**, *96*, 022511. [[CrossRef](#)]
27. Neukermans, S.; Janssens, E.; Tanaka, H.; Silverans, R.E.; Lievens, P. Element- and Size-Dependent Electron Delocalization in Au_NX⁺ Clusters (X = Sc, Ti, V, Cr, Mn, Fe, Co, Ni). *Phys. Rev. Lett.* **2003**, *90*, 033401. [[CrossRef](#)]
28. Ferrari, P.; Vanbuel, J.; Janssens, E.; Lievens, P. Tuning the Reactivity of Small Metal Clusters by Heteroatom Doping. *Acc. Chem. Res.* **2018**, *51*, 3174. [[CrossRef](#)] [[PubMed](#)]
29. Neumaier, M.; Weigend, F.; Hampe, O.; Kappes, M.M. Reactions of mixed silver-gold cluster cations Ag_mAu_n⁺ (m + n = 4, 5, 6) with CO: Radiative association kinetics and density functional theory computations. *J. Chem. Phys.* **2006**, *125*, 104308. [[CrossRef](#)]
30. Vanbuel, J.; Fernández, E.M.; Ferrari, P.; Gewinner, S.; Schöllkopf, W.; Balbás, L.C.; Fielicke, A.; Janssens, E. Hydrogen Chemisorption on Singly Vanadium-Doped Aluminum Clusters. *Chem. Eur. J.* **2017**, *23*, 15638–15643. [[CrossRef](#)]
31. Medel, V.M.; Reber, A.C.; Chauhan, V.; Sen, P.; Köster, A.M.; Calaminici, P.; Khanna, S.N. Nature of Valence Transition and Spin Moment in Ag_nV⁺ Clusters. *J. Am. Chem. Soc.* **2014**, *136*, 8229–8236. [[CrossRef](#)]
32. Janssens, E.; Neukermans, S.; Wang, X.; Veldeman, N.; Silverans, R.E.; Lievens, P. Stability patterns of transition metal doped silver clusters: Dopant- and size-dependent electron delocalization. *Eur. Phys. J. D* **2005**, *34*, 23–27. [[CrossRef](#)]
33. Kaydashev, V.; Ferrari, P.; Heard, C.; Janssens, E.; Johnston, R.L.; Lievens, P. Optical Absorption of Small Palladium-Doped Gold Clusters. *Part. Part. Syst. Charact.* **2016**, *33*, 364–372. [[CrossRef](#)]
34. Jia, M.; van der Tol, J.; Li, Y.; Chernyy, V.; Bakker, J.M.; Pham, L.N.; Nguyen, M.T.; Janssens, E. Structures and magnetic properties of small Co_n⁺ and Co_{n-1}Cr⁺ (n = 3–5) clusters. *J. Phys. Condens. Matter* **2018**, *30*, 474002. [[CrossRef](#)]
35. Ferrari, P.; Hussein, H.A.; Heard, C.J.; Vanbuel, J.; Johnston, R.L.; Lievens, P.; Janssens, E. Effect of palladium doping on the stability and fragmentation patterns of cationic gold clusters. *Phys. Rev. A* **2018**, *97*, 052508. [[CrossRef](#)]
36. Ferrari, P.; Vanbuel, J.; Li, Y.; Liao, T.-W.; Janssens, E.; Lievens, P. Modifications of gas aggregation sources: The double laser ablation source approach. In *Gas Aggregation Synthesis of Nanoparticles*, 1st ed.; Huttel, Y., Ed.; Wiley-VCH: Weinheim, Germany, 2017; pp. 59–78. ISBN 978-3-527-34060-6.

37. Duncan, M.A. Invited Review Article: Laser vaporization cluster sources. *Rev. Sci. Instrum.* **2012**, *83*, 041101. [[CrossRef](#)] [[PubMed](#)]
38. Geusic, M.E.; Jarrold, M.F.; McIlrath, T.J.; Freeman, R.R.; Brown, W.L. Photodissociation of carbon cluster cations. *J. Chem. Phys.* **1987**, *86*, 3862. [[CrossRef](#)]
39. Hansen, K.; Herlert, A.; Schweikhard, L.; Vogel, M. Dissociation energies of gold clusters Au_N^+ , $N = 7-27$. *Phys. Rev. A* **2006**, *73*, 063202. [[CrossRef](#)]
40. Ferrari, P.; Hansen, K.; Lievens, P.; Janssens, E. Stability of small cationic platinum clusters. *Phys. Chem. Chem. Phys.* **2018**, *20*, 29085–29090. [[CrossRef](#)] [[PubMed](#)]
41. Neese, F. The ORCA program system. *Wiley Interdiscip. Rev. Comput. Mol. Sci.* **2012**, *2*, 73–78. [[CrossRef](#)]
42. Lu, P.; Kuang, X.Y.; Mao, A.J.; Wang, Z.H.; Zhao, Y.R. Structural and electronic properties of silver-doped gold clusters Au_nAg^v ($2 \leq n \leq 10$; $v = 0, \pm 1$): Comparison with pure gold clusters. *Mol. Phys.* **2011**, *109*, 2057–2068. [[CrossRef](#)]
43. Weis, P.; Welz, O.; Vollmer, E.; Kappes, M.M. Structures of mixed gold-silver cluster cations ($Ag_mAu_n^+$, $m + n < 6$): Ion mobility measurements and density-functional calculations. *J. Chem. Phys.* **2004**, *120*, 677. [[CrossRef](#)]
44. Shayeghi, A.; Johnston, R.L.; Rayner, D.M.; Schfer, R.; Fielicke, A. The Nature of Bonding between Argon and Mixed Gold–Silver Trimers. *Angew. Chem. Int. Ed.* **2015**, *54*, 10675. [[CrossRef](#)] [[PubMed](#)]
45. Shayeghi, A.; Schäfer, R.; Rayner, D.M.; Johnston, R.L.; Fielicke, A. Charge-induced dipole vs. relativistically enhanced covalent interactions in Ar-tagged Au–Ag tetramers and pentamers. *J. Chem. Phys.* **2015**, *143*, 024310. [[CrossRef](#)]
46. Weigenda, F.; Ahlrichs, R. Balanced basis sets of split valence, triple zeta valence and quadruple zeta valence quality for H to Rn: Design and assessment of accuracy. *Phys. Chem. Chem. Phys.* **2005**, *7*, 3297–3305. [[CrossRef](#)]
47. Pyykko, P. Relativistic effects in structural chemistry. *Chem. Rev.* **1988**, *88*, 563–594. [[CrossRef](#)]
48. Van Wüllen, C. Molecular density functional calculations in the regular relativistic approximation: Method, application to coinage metal diatomics, hydrides, fluorides and chlorides, and comparison with first-order relativistic calculations. *J. Chem. Phys.* **1998**, *109*, 392. [[CrossRef](#)]
49. Pantazis, D.A.; Chen, X.-Y.; Landis, C.R.; Neese, N. All-Electron Scalar Relativistic Basis Sets for Third-Row Transition Metal Atoms. *J. Chem. Theory Comput.* **2008**, *4*, 908–919. [[CrossRef](#)]
50. Häkkinen, H.; Landman, U. Gold clusters (Au_N , $2 < N < 10$) and their anions. *Phys. Rev. B* **2000**, *62*, R2287. [[CrossRef](#)]
51. Massen, C.; Mortimer-Jones, T.V.; Johnston, R.L. Geometries and segregation properties of platinum–palladium nanoalloy clusters. *J. Chem. Soc. Dalton Trans.* **2002**, *0*, 4375–4388. [[CrossRef](#)]
52. Martínez, J.I.; Alonso, J.A. An improved descriptor of cluster stability: Application to small carbon clusters. *Phys. Chem. Chem. Phys.* **2018**, *20*, 27368–27374. [[CrossRef](#)]
53. Koyasu, K.; Mitsui, M.; Nakajima, A.; Kaya, K. Photoelectron spectroscopy of palladium-doped gold cluster anions; Au_nPd^- ($n = 1-4$). *Chem. Phys. Lett.* **2002**, *358*, 224–230. [[CrossRef](#)]
54. Janssens, E.; Tanaka, H.; Neukermans, S.; Silverans, R.E.; Lievens, P. Two-dimensional magic numbers in mass abundances of photofragmented bimetallic clusters. *New J. Phys.* **2003**, *5*, 46.1–46.10. [[CrossRef](#)]
55. Ferrighi, L.; Hammer, B.; Madsen, G.K.H. 2D–3D Transition for Cationic and Anionic Gold Clusters: A Kinetic Energy Density Functional Study. *J. Am. Chem. Soc.* **2009**, *131*, 10605–10609. [[CrossRef](#)] [[PubMed](#)]
56. Van der Tol, J.; Jia, D.; Li, Y.; Chernyy, V.; Bakker, J.M.; Nguyen, M.T.; Lievens, P.; Janssens, E. Structural assignment of small cationic silver clusters by far-infrared spectroscopy and DFT calculations. *Phys. Chem. Chem. Phys.* **2017**, *19*, 19360–19368. [[CrossRef](#)] [[PubMed](#)]
57. Harding, D.J.; Kerpál, C.; Rayner, D.M.; Fielicke, A. Communication: The structures of small cationic gas-phase platinum clusters. *J. Chem. Phys.* **2012**, *136*, 211103. [[CrossRef](#)] [[PubMed](#)]
58. Xing, X.; Hermann, A.; Kuang, X.; Ju, M.; Lu, C.; Jin, Y.; Xia, X.; Maroulis, G. Insights into the geometries, electronic and magnetic properties of neutral and charged palladium clusters. *Sci. Rep.* **2016**, *6*, 19656. [[CrossRef](#)] [[PubMed](#)]
59. Vogel, M.; Hansen, K.; Herlert, A.; Schweikhard, L. Decay pathways of small gold clusters. *Eur. Phys. J. D* **2001**, *16*, 73–76. [[CrossRef](#)]

